## Malaysian Journal of Analytical Sciences (MJAS)



Published by Malaysian Analytical Sciences Society

## MAGNETIC NANOPARTICLE FOR REMOVING SUNSET YELLOW DYE: TAGUCHI OPTIMIZATION

(Zarah Nano Magnetit untuk Penyingkiran Pewarna Kuning Matahari Terbenam: Pengoptimuman Taguchi)

Nurina Izzah Mohd Husani<sup>1</sup>, Nur Amani Izzati Mohamad Hisham<sup>2</sup>, Nor Munira Hashim<sup>1</sup>, Clayrine Shima Anak Lasu<sup>1</sup>, Noorfatimah Yahaya<sup>1</sup>, Muggundha Raoov<sup>3</sup>, and Nur Nadhirah Mohamad Zain<sup>1</sup>\*

<sup>1</sup>Department of Toxicology, Advanced Medical And Dental Institute, Universiti Sains Malaysia,
13200 Kepala Batas, Penang, Malaysia

<sup>2</sup>Faculty of Science and Technology, Universiti Sains Islam Malaysia, Bandar Baru Nilai,
71800, Nilai, Negeri Sembilan, Malaysia

<sup>3</sup>Department of Chemistry, Faculty of Sciences, Universiti Malaya, 50603 Kuala Lumpur, Malaysia

\*Corresponding author: nurnadhirah@usm.my

Received: 9 March 2022; Accepted: 30 May 2023; Published: 22 August 2023

#### **Abstract**

This study describes the role of magnetite nanoparticle (MNP) or Fe<sub>3</sub>O<sub>4</sub>, which are magnetic nanomaterials (MNMs), as adsorbents for the removal of a synthetic azo dye called sunset yellow FCF (SY) from aqueous samples. Improper release of the SY dye into water can have significant adverse effects on the environmental, including disruption of photosynthesis, obstructs sunlight penetration, and risks to aquatic life and human health. Therefore, it is crucial to develop effective methods for removing the SY dye from water sources. This research aims to investigate the potential of Fe<sub>3</sub>O<sub>4</sub> magnetic nanoparticles in removing the SY dye from water samples. By analyzing the effects of Fe<sub>3</sub>O<sub>4</sub> nanoparticles, this study aims to provide insights into their efficiency and effectiveness as a potential solution for the removal of the SY dye, contributing to the development of sustainable water treatment strategies. The adsorbents was prepared using co-precipitation method, and their characteristics were analyzed using various instruments. Furthermore, the study investigated the adsorption conditions, including the optimization of pH, adsorbent dosage, and contact time using the Taguchi optimization method. The optimization for the effect of temperature and initial concentration of dye was conducted separately. The results of this study showed that the interaction between the homogenous surface of the adsorbents and the adsorbates or analytes molecules involved chemisorption and monolayer adsorption. The adsorption was found to be feasible, spontaneous, increased randomness, and endothermic. Additionally, the prepared adsorbents were validated by applying to remove the SY dye from three actual wastewater samples. The removal percentage ranged approximately from 30% to 85% with a low relative standard deviation (RSD% < 9.2%). This demonstrated that the adsorbents remained reliable for removing the dye from real samples were spiked with a high concentration of analytes. Overall, this study presents a promising approach for removing the SY dye from wastewater samples. It shows that even the bare form of MNMs base can be extensively developed for analyte removal from real aqueous samples.

Keywords: magnetic nanoparticles, sunset yellow dye FCF, Taguchi optimization, adsorption, wastewater

### Mohd Husani et al.: MAGNETIC NANOPARTICLE FOR REMOVING SUNSET YELLOW DYE: TAGUCHI OPTIMIZATION

#### Abstrak

Artikel ini menerangkan peranan zarah nano magnetit (MNP) atau Fe<sub>3</sub>O<sub>4</sub>, yang merupakan bahan nano magnetik (MNMs), sebagai bahan jerap untuk menyingkirkan pewarna azo sintetik yang dipanggil kuning matahari terbenam FCF (SY) daripada sampel berakua. Pembebasan pewarna SY yang tidak betul ke dalam air boleh memberi kesan buruk yang ketara kepada alam sekitar, termasuk gangguan fotosintesis, menghalang penembusan cahaya matahari, dan risiko kepada hidupan akuatik serta kesihatan manusia. Oleh itu, adalah penting untuk membangunkan kaedah yang berkesan untuk mengeluarkan pewarna SY daripada sumber air. Penyelidikan ini bertujuan untuk menyiasat potensi nanopartikel magnet Fe<sub>3</sub>O<sub>4</sub> dalam menyingkirkan pewarna SY daripada sampel air. Dengan menganalisis kesan nanopartikel Fe<sub>3</sub>O<sub>4</sub>, kajian ini bertujuan untuk memberikan pandangan tentang kecekapan dan keberkesanannya sebagai penyelesaian yang berpotensi untuk penyingkiran pewarna SY, menyumbang kepada pembangunan strategi rawatan air yang mampan. Bahan jerap telah disediakan menggunakan kaedah pemendakan bersama, dan ciri-cirinya dianalisis dengan menggunakan pelbagai instrumen. Tambahan pula, kajian ini menyiasat keadaan penjerapan, termasuk pengoptimuman pH, dos penjerap, dan masa sentuhan menggunakan kaedah pengoptimuman Taguchi. Pengoptimuman untuk kesan suhu dan kepekatan awal pewarna dijalankan secara berasingan. Hasil kajian ini menunjukkan bahawa interaksi antara permukaan homogen bahan jerap dan bahan dijerap atau molekul analit melibatkan penjerapan kimia dan monolapisan. Penjerapan didapati tersaur, spontan, peningkatan kerawakan, dan endoterma. Tambahan pula, bahan jerap yang disediakan telah disahkan potensinya dengan menggunakannya untuk menyingkirkan pewarna SY daripada tiga sampel air buangan sebenar. Peratusan penyingkiran berjulat kira-kira dari 30% hingga 85% dengan sisihan piawai relatif rendah (RSD% < 9.2%). Ini menunjukkan bahawa bahan jerap kekal boleh dipercayai untuk menyingkirkan pewarna daripada sampel sebenar yang telah dicemari dengan kepekatan analit yang tinggi. Secara keseluruhan, kajian ini membentangkan pendekatan yang menjanjikan dalam mengeluarkan pewarna SY daripada sampel air buangan. Ia menunjukkan bahawa walaupun bentuk yang asas MNMs dapat dibangunkan secara meluas untuk penyingkiran analit daripada sampel berakua sebenar.

Kata kunci: zarah nano magnetit, pewarna kuning matahari terbenam FCF, pengoptimuman Taguchi, penjerapan, air kumbahan

#### Introduction

In this modern world, rapid industrialization has led to a gradual increase in environmental pollution [1]. Among the various types of pollution, water pollution is particularly concerning. Water is not only essential for human body, it is also crucial for human daily activities such as agriculture, industrial production, and drinking water [2, 3, 4]. Unfortunately, the scarcity of clean water caused by pollution erodes all these benefits. Water pollution occurs mainly due to the discharge of emerging contaminants (EC) from various industries, such as heavy metals, pesticides, polyaromatic hydrocarbons, and dyes, as highlighted Belachew et al. [5]. This problem needs to be addressed urgently to ensure that the water sources can be preserved and the maintained for healthy environment. Through the implementation of stringent regulations and effective strategies, water pollution can be prevented and its quality can be restored.

Dyes, as one type of EC, are colorants that can be transferred from a liquid onto numerous substrates and are usually used in industries such as printing, textile, plastics, rubbers, and foodstuffs [6, 7]. They are also popular as food colorants in the food industry to enhance

taste and to improve the appearance of food. Food colorants are broadly classified into two categories which are natural colorants and synthetic colorants. Due to their excellent stability, effectiveness, and low-cost production, synthetic colorants are extensively used in the industry [8]. Natural dyes are produced from various sources, such as animal, plant, and mineral deposits. The commonly used natural dyes include brown (caramel), yellow (turmeric), and red (beet juice). On the other hand, the synthetic dyes, which are produced through chemical processes, offer a wider variety of colors. Some of these dyes include Sunset Yellow, Allura Red, Brilliant Blue, and Tartrazine[9].

One specific synthetic azo dye, Sunset Yellow FCF (SY), known as CI Food Yellow 3, INS No.110 and Orange Yellow S, has the chemical name disodium 2-hydroxy-1-(4-sulphonatophenylazo)naphtha-lene-6-sulphonate [8]. SY in the form of powder present as orange-red colour and is soluble in water. It used in pharmaceuticals, cosmetics, and food products [10]. In the food industry, SY is commonly used to produce apricot jam, lemon curd, sweets, beverage mixes, custard powders, and instant noodles [11]. Apparently,

this type of synthetic dye is beneficial in many fields, especially in the food industry.

However, despite its usefulness in various fields, it still has limitations, especially when released abundantly into water without pre-treatment. This can affect the water ecosystem and human beings, as they are interconnected through the food chain and food web. Nwuzor et al. mentioned that some dyes are lost in streams during the industrial colouring process, and these dyes are toxic and can disrupt the water's nature state by hindering sunlight penetration, disrupting photosynthesis, and causing aesthetic issues. Furthermore, they can cause allergies and affect neurobehavioral and reproductive parameters, leading to symptoms such as diarrhea and allergies [11]. Therefore, the presence of dyes like SY as water effluents without proper treatment could have a negative impact on aquatic organisms and human health.

Therefore, remedies should be outlined to curb this issue. According to a previous study by Villar Blanco et al., three forms of techniques can be implemented including physicochemical, physical, and biological. Several actions such as oxidation, ion exchange, flocculation, filtration, ozonation, membrane separation, precipitation, and adsorption have been employed to treat the issue. However, most of these processes encountered some limiting factors, such as high operating costs, difficulties in timing implementation, and the generation of toxic by-products and sludges [14, 15]. As a result, many of them cannot be efficiently utilized. However, Jeeva et al. stated that adsorption is the most efficient method to treat effluents due to its simplicity, cost-effectiveness, and directness. It is extensively applied to remove pollutants from wastewater as it exhibits high removal efficiency [16].

Adsorption is a process that involves the accumulation of molecules on the surface or at the interface between two phases [17]. It is also known as a separation process in which molecules tend to accumulate on the surface of the adsorbent due to the presence of attractive forces, such as the Van der Waals force. This accumulation creates an adsorbate film on the adsorbent's surface [18]. Thus, it is evident that the adsorbate and adsorbent

are essential elements in an adsorption process, highlighting the importance of choosing a suitable adsorbent to ensure the effective adsorption of the targeted analyte (adsorbate) [19].

Recently, magnetic nanoparticles, such as iron oxide (Fe<sub>3</sub>O<sub>4</sub>), have been recognized as effective adsorbents for pollutants' removal in recent years. Previous studies have validated the use of Fe<sub>3</sub>O<sub>4</sub> in developing a simple, inexpensive, and efficient adsorption method [20]. Fe<sub>3</sub>O<sub>4</sub>, also known as magnetite or magnetic nanoparticles (MNPs), is derived from nanomaterials (NMs). NMs are generally small-sized materials ranging from 1 to 100 nm [21]. These characteristics contributed to their larger surface area and unique properties, making them ideal sorbents.

Furthermore, the use of MNPs derived from NMs is favored due to their susceptibility to external magnetic fields. This property eliminates the need for cumbersome processes like centrifugation and filtration, as the sorbents can be easily and quickly separated from the liquid reaction system using a magnet [22]. As a result, the adsorption or removal of analytes (such as dyes) from water samples becomes straightforward and accessible. Importantly, aforementioned benefits highlight that Fe<sub>3</sub>O<sub>4</sub> can be implemented to enhance the adsorption process of various analytes, including dyes.

Based on the preceding discussion, the main objective of this study was to investigate the performance of Fe<sub>3</sub>O<sub>4</sub> in removing a synthetic azo dye, sunset yellow FCF (SY), from water samples. The study involved optimizing several parameters that influenced the removal performance of SY, such as pH, contact period, temperature, adsorbent dosage, and initial concentration of SY. The application of the Taguchi method in designing the optimization study was also examined. Furthermore, the study explored the kinetics reaction and isotherm adsorption of Fe<sub>3</sub>O<sub>4</sub> in removing SY from an aqueous solution to understand the adsorption mechanism. Additionally, a thermodynamics study was conducted to assess the viability and spontaneity of the process. Finally, the optimized values were applied to

real water to validate the performance of the proposed method for practical sample analysis.

#### **Materials and Methods**

#### Chemicals and reagents

Ferrous chloride tetrahydrate (FeCl<sub>2</sub>.4H<sub>2</sub>O) and ferric chloride hexahydrate (FeCl<sub>3</sub>.6H<sub>2</sub>O) from R&M Chemicals (Edmonton, Canada) were used to synthesize the MNPs, Fe<sub>3</sub>O<sub>4</sub>. Methanol was supplied by HmbG Chemicals (Cologne, Germany), and a 25% ammonia solution (NH<sub>3</sub>) utilized was from Merck, Darmstadt, Germany. The Sunset Yellow FCF powder was purchased from R&M Marketing (Essex, U.K.). All reagents and chemicals were used without further purification.

#### Instrumentation

The experiments were conducted using deionized water obtained from the Sartorius Stedim deionized water dispenser, Milli–Q® system (Arium 611 DI). A pH meter (BP3001 Trans Instruments) was utilized for measuring and adjusting the pH value. A UV-vis spectrophotometer (Perkin Elmer Lambda25) was employed to determine residual concentrations of the Sunset Yellow FCF at  $\lambda_{max} = 480.9$  nm. An incubator shaker (IKA, KS4000 control) was used to shake the sample solution at 300 rpm with adjustable temperature and time, while mechanical shaker (Orbitron) was used to shake the solution at a similar speed and at room temperature with adjustable time.

#### Synthesis of Fe<sub>3</sub>O<sub>4</sub>

In this study, Fe<sub>3</sub>O<sub>4</sub> was prepared using a conventional co-precipitation method with slight modification [23]. Firstly, FeCl<sub>2</sub>.4H<sub>2</sub>O and FeCl<sub>3</sub>.6H<sub>2</sub>O were mixed and dissolved in 50 mL of deionized water. Then, the mixture was stirred under nitrogen gas at 50°C for 30 min. Subsequently, ammonia solution (25%) was added into the mixture solution to allow the magnetization process, and the mixture was agitated for an hour at 90°C under nitrogen gas before the final products were collected by an external magnet, followed by washing step using 50 mL methanol and 50 mL deionized water alternately for several times. Afterward, the products were dried in an oven overnight. Finally, the dried products were crushed and ground using a pestle and

mortar, before stored for further use.

#### Characterization of the synthesized Fe<sub>3</sub>O<sub>4</sub>

For the characterization process, several instruments were employed to examine the physical characteristics of the synthesized Fe<sub>3</sub>O<sub>4</sub>. A vibrating sample magnetometer (VSM, model Lake Shore/7404, McCourkle Boulevard, WO, USA) was used to investigate the magnetic properties of the adsorbent. Fourier transform-infrared spectroscopy (FT-IR) with the KBr technique from model Thermo Nicolet model in Waltham, USA, and thermogravimetric analysis (TGA, model Perkin Elmer) was utilized to identify the functional groups and the thermal stability of Fe<sub>3</sub>O<sub>4</sub>, respectively. The morphology of the synthesized Fe<sub>3</sub>O<sub>4</sub> was examined using a transmission electron microscope (TEM, Phillips CM12 Version 3.2 model, Hillsboro, USA) and a scanning electron microscope (SEM, QUANTA FEG650 model, Hillsboro, Oregon, USA). X-ray diffractometer (XRD) from Siemens D5000 model (Frimley, UK) was applied for the phase identification of adsorbent crystallinity and unit cell dimension. Additionally, Brunauer-Emmet-Teller (BET) analysis was conducted using Quantachrome model (Boynton Beach, FL, USA) to measure the surface area of the adsorbent and determine the physical adsorption of gas particles on a solid surface. Prior to BET analysis, the prepared adsorbent was degassed at 80°C for 2 h to remove moisture.

#### **Adsorption experiments**

All the adsorption experiments were conducted using a 20 mL glass vial containing a specific amount of Fe<sub>3</sub>O<sub>4</sub> adsorbent mixed with 10 mL of a sample solution containing a predetermined concentration of SY dye as the analyte. The vials were then placed on an incubator or a mechanical shaker at designated temperature for a specific duration at a consistent speed of 300 rpm. The adsorption experiments were carried out by varying different parameters, including pH (2.0, 3.0, 4.0, and 5.0), contact period (10, 20, 30, and 40 min), adsorbent dosage (5, 10, 15, and 20 mg), temperature (298, 313, and 333 K) and initial concentration of SY dye (5, 10, 20, 40, and 60 ppm).

During the experiment, the pH of the solution was

adjusted by adding hydrochloric acid, HCl (0.1 M), or sodium hydroxide, NaOH (0.1 M). After adsorption, Fe<sub>3</sub>O<sub>4</sub> adsorbents were separated using an external magnet, and the remaining solutions were analyzed

using a UV-vis spectrophotometer at  $\lambda_{max}$ = 480.9 nm. All the experiments were conducted in triplicate. Finally, the percentage removal (R%) of each run was calculated by using equation (1):

$$R (\%) = \frac{\text{Co-Ce}}{\text{Co}} \times 100\%$$
 (1)

where  $C_0$  refers to the initial concentration of the dye and  $C_e$  refers to the equilibrium concentration of the SY FCF dye (ppm).

#### **Optimization for adsorption experiments**

In this study, two methods were employed to conduct the optimization. The optimization for the effects of pH, contact period, and adsorbent dosage was performed using the Taguchi Orthogonal Array design. Several values were selected for each factor (pH, contact period, and adsorbent dosage), and the experiments were conducted based on the pre-designed data. Additionally, the values for the initial concentration of SY and temperature were predetermined and kept constant for the Taguchi experiment.

Subsequently, separate procedures were conducted at various initial concentrations of SY and different temperatures to optimize the effect of initial concentration and temperature. During these runs, the pH value, adsorbent dosage, and contact period were maintained constant at pH 3, 10 mg, and 10 min, respectively. These values were then optimized based on the outcomes of the Taguchi experiment.

#### Taguchi method for optimization

The Taguchi method is an effective strategy for designing an experiment to obtain the optimum process results, which was proposed by Dr. Genichi Taguchi [24]. It is a method that combines multiple factors at various levels while ensuring equal consideration of all levels of each factor, thereby reducing the number of experimental runs. To conduct the Taguchi method, several procedures were adopted during the process.

According to Nandhini et al. (2014), the three main procedures adopted in designing parameters using the Taguchi method are as follows: (1) experimental planning, which involves the selection of factors (*P*), their values (levels, *L*) and the appropriate Taguchi orthogonal array design, (2) implementation of the experimental design based on the designed table, and (3) analysis of results using Analysis of Variance (ANOVA), main effect plot of signal-to-noise (S/N) ratio, and means to determine the optimum value for the control factors [25].

In this study, the three main procedures were adopted. The Taguchi method was conducted at varying ranges of controllable factors, namely pH (2.0, 3.0, 4.0, and 5.0), contact period (10, 20, 30, and 40 min), and adsorbent dosage (5, 10, 15, and 20 mg). Simultaneously, the initial concentration and temperature were fixed at 10 ppm (10 mL) and room temperature, respectively. Since there were three factors (P) with four testing conditions values (L) for each factor, the Taguchi experiment was conducted by implementing Taguchi design:  $L_{16}$  (P=3, L=4). Table 1 below shows the selected parameters for this study. Meanwhile, Table 2 shows the experimental plan based on  $L_{16}$  (P=3, L=4) design, and Table 3 depicts the experimental runs with the actual values of testing conditions for each run. Signal to noise ratio and the implementation of ANOVA were also observed to determine the optimum conditions and assess the contribution of each factor sequentially.

Table 1. Selected experimental factors and their corresponding values at different levels

Symbol	Factors	Units	Levels				
Symbol	1 actors	Chits	1	2	3	4	
A	рН	-	2	3	4	5	
В	Contact period	min	10	20	30	40	
C	Adsorbent dosage	mg	5	10	15	20	

Table 2. 16 runs based on Taguchi design L16 (P=3, L=4)

		Factors and Their Levels					
No. of Run	pН	Contact Period	Adsorbent Dosage				
1	1	1	1				
2	1	2	2				
3	1	3	3				
4	1	4	4				
5	2	1	2				
6	2	2	1				
7	2	3	4				
8	2	4	3				
9	3	1	3				
10	3	2	4				
11	3	3	1				
12	3	4	2				
13	4	1	4				
14	4	2	3				
15	4	3	2				
16	4	4	1				

Table 3. 16 runs of Taguchi optimization experiment and their respective testing conditions values

No. of Run	pН	Contact Period	Adsorbent Dosage
1	2	10	5
2	2	20	10
3	2	30	15
4	2	40	20
5	3	10	10
6	3	20	5
7	3	30	20
8	3	40	15
9	4	10	15
10	4	20	20
11	4	30	5
12	4	40	10
13	5	10	20
14	5	20	15
15	5	30	10
16	5	40	5

### Optimization for the effect of temperature and initial concentration

This study was conducted using various initial concentrations of SY (5, 10, 20, 40, and 60 ppm) in 10 mL of sample solution at different temperatures of 298, 313, and 333 K, separately. Meanwhile, other factors such as pH value, contact period, and adsorbent dosage were fixed at their optimized values obtained from the Taguchi experiment: pH 3, 10 min, and 10 mg, respectively.

### Adsorption isotherm, kinetic, and thermodynamic study

To further investigate the reaction mechanism and adsorbent behaviour toward the analyte, detailed evaluation of kinetic, isotherm, and adsorption thermodynamics were conducted. The behaviour of Fe<sub>3</sub>O<sub>4</sub> toward SY dye was studied using several well-

$$\log (q_e - q_t) = \log q_e - \frac{k1}{2.303} t \tag{2}$$

The pseudo-second order model is another well-known kinetic model. This model has been implemented in several sorption systems to successfully examine chemisorption interactions, which includes the exchange of electrons and valance sharing between the

$$\frac{t}{q_1} = \frac{1}{k_2 q_e^2} + \frac{t}{q_e} \tag{3}$$

where  $q_e$  and  $q_t$  (mg/g) represent the amount of SY FCF dye adsorbed at equilibrium and at time t (min), respectively.  $k_1$  (min<sup>-1</sup>) is the rate constant for the first order adsorption, and  $k_2$  (g/mg.min) is rate constant for the second order adsorption.

Furthermore, the suitability of the model to determine adsorption kinetics was also assessed by calculating the normalized standard deviation  $\Delta q$  (%) and relative error (%) based on equations (4) and (5), respectively:

adsorbent and analyte [23, 28]. For this study, the

determination of kinetic behavior using the pseudo-

second order model was expressed by the following

linear equation, equation (3):

$$\Delta q \, (\%) = \sqrt{\frac{((q_{\rm exp} - q_{\rm cal})/q_{\rm exp})^2}{N-1}} \, x \, 100$$
 (4)

Relative error (%) = 
$$\left(\frac{q_{exp} - q_{cal}}{q_{exp}}\right)$$
 (5)

where N represents the number of data points, while  $q_{exp}$  and  $q_{cal}$  represent the experimental and calculated adsorption capacities, respectively.

known models. The thermodynamic study was then investigated using entropy ( $\Delta S^{\circ}$ ), enthalpy ( $\Delta H^{\circ}$ ), and free Gibbs energy ( $\Delta G^{\circ}$ ).

#### Adsorption kinetics study

The use of kinetic model in a study can evaluate the sorption mechanism and potential rate-determining steps [23, 26]. In this study, two models were utilized to investigate the kinetic behavior of Fe<sub>3</sub>O<sub>4</sub> toward SY dye: the pseudo-first order and pseudo-second order. The pseudo-first order model is a kinetic model that was proposed Lagergren in 1898, and it is the most commonly employed kinetic model for liquid-solid adsorption systems [15, 27]. To pursue this study on SY adsorption onto Fe<sub>3</sub>O<sub>4</sub> adsorbent, the pseudo-first order model was described based on pseudo-first order linear equation, equation (2):

#### Adsorption isotherms study

Adsorption isotherm models are crucial for predicting and comparing the performance of an adsorption process [29]. In this study, five isotherm models were implemented to investigate the adsorption of SY dye onto Fe<sub>3</sub>O<sub>4</sub>. The models used were Langmuir, Freundlich, Dubinin-Radusckich, Halsey, and Temkin isotherm models.

$$\frac{C_e}{q_e} = \frac{1}{q_m} \cdot C_e + \frac{1}{b \cdot q_m}$$
 (6)

(7), respectively.

$$\log q_{\rm e} = \frac{1}{n} \log C_{\rm e} + \log K_{\rm F} \tag{7}$$

 $C_e$  (mg.L<sup>-1</sup>) represents the initial concentration of the adsorbate according to the Langmuir model and the concentration at equilibrium according to the Freundlich model.  $q_e$  (mg.g<sup>-1</sup>) represents the amount of adsorbate adsorbed at equilibrium. The Langmuir model is characterized by the parameters  $q_m$  (mg.g<sup>-1</sup>) and b (L.mg<sup>-1</sup>), which represent the maximum adsorption capacity and the rate of adsorption, respectively. The Freundlich model is characterized by the parameters  $K_F$  (mg.g<sup>-1</sup>) and n, which represent the adsorption capacity and intensity, respectively.

The Dubinin-Radusckich model is generally used to express the adsorption mechanism with Gaussian energy

The Langmuir model is an empirical model that assumes

a homogenous surface of the adsorbent and involves

monolayer adsorption, with the adsorbed layer having a

thickness of one molecule [23, 29], while the Freundlich

isotherm model is an empirical model which generally

used to illustrate heterogeneous adsorbents data. In this

study, the Langmuir and Freundlich model parameters

were described through their linear equations (6) and

onto heterogeneous surfaces [30], while the Halsey

model is suitable for multilayer adsorption and illustrates the heterosporous nature of a material [31].

Additionally, the Temkin is an empirical isotherm

model that considers the interactions between adsorbent

and adsorbate while neglecting the concentration values,

 $ln q_e = ln q_m - \beta E^2$  (8)

$$E = RT \ln \left[1 + \frac{1}{C_c}\right] \tag{9}$$

$$\ln q_{\rm e} = \left[ \frac{1}{n} \ln K_{\rm H} \right] - \frac{1}{n} \ln C_{\rm e} \tag{10}$$

$$q_e = \beta \ln K_T + \beta \ln C_e \tag{11}$$

The adsorption energy constant, denoted by  $\beta$ , can be calculated using the Dubinin-Radusckich equation. Additionally,  $\beta$  is equal to  $\frac{RT}{b_{\tau}}$  at a given temperature (T in Kelvin), which corresponds to the Temkin equation. The universal gas constant, represented by R, is measured in units of kJ.mol<sup>-1</sup>. The Halsey isotherm constants, denoted as  $K_H$  and n, are obtained from the

slope and intercept of the ln  $q_e$  against ln  $C_e$ , respectively. The Temkin constant, KT, is related to the equilibrium binding energy, and  $b_{\tau}$  is associated with the heat of adsorption.

#### Adsorption thermodynamic

isotherm models, respectively.

Thermodynamics must be considered in adsorption

experiments to demonstrate the viability and spontaneity of the process [23]. Thermodynamic parameters can be determined in an adsorption process as they are temperature-dependent [32]. In this research, the effects of temperature on the thermodynamic parameters such as  $\Delta H^{\circ}$ ,  $\Delta S^{\circ}$ , and  $\Delta G^{\circ}$  were investigated at three

different temperatures (298, 313, and 333 K). Subsequently, the Van Hoff plot was obtained by plotting ln  $k_d$  against 1/T based on equation (12). The slope of the curve was used to calculate  $\Delta H^{\circ}$ , while  $\Delta S^{\circ}$  was determined the y-intercept.

$$ln~k_d = -\frac{\Delta H^\circ}{RT} + \frac{\Delta S^\circ}{R}$$

The equilibrium constant, which represents the ratio of the forward and reverse reaction rates at equilibrium, is denoted by  $k_{\text{d}}$ .

#### Pre-treatment of real samples

Wastewater samples were randomly collected from various industrial areas around the Kepala Batas area (5.5172° N, 100.4315° E). All samples were filtered using a nylon filter and stored in appropriate containers before use.

#### Method validation and real sample analysis

To validate the proposed method, linearity, and repeatability (intra-day and inter-day) were evaluated

$$SD = \sqrt{\frac{\sum (\bar{x} - x)^2}{n-1}}$$
 (13)

$$RSD = \frac{SD}{\bar{x}} \times 100 \tag{14}$$

In a set of measurements with a sample size of n, where  $\bar{x}$  represents the mean and x represents the result of each individual run, the standard deviation (SD) is a measure of the spread or variability of the data.

To assess the reliability of the proposed method, three real samples were spiked with three different analyte concentrations and analyzed using a UV-vis spectrophotometer. The analysis aimed to investigate the matrix effect on the removal of SY by  $Fe_3O_4$ .

#### **Results and Discussion**

#### Characterization of the adsorbent

FTIR analysis was conducted to identify the vibration of functional groups present on the surface of the prepared Fe<sub>3</sub>O<sub>4</sub>. The FTIR spectrum of Fe<sub>3</sub>O<sub>4</sub> is shown in Figure

under optimized conditions. The linearity of SY in water samples was assessed by constructing a calibration curve ranging from 2 to 80 ppm. The coefficient of determination (R<sup>2</sup>) value was obtained from a linear plot of absorbance (A) versus analyte concentration (ppm).

(12)

Accuracy (removal) and precision (relative standard deviation, RSD%) were assessed by analyzing effluent wastewater samples with a spiked standard solution at three different concentration levels (5, 20, and 60 ppm). Equation (1) was used to calculate accuracy, while equations (13) and (14) were employed to calculate the precision.

1, and the data are presented in Table 4. Based on the figure, two prominent peaks were in the spectrum of Fe<sub>3</sub>O<sub>4</sub>. A strong and broad peak was identified at 3417.6 cm<sup>-1</sup>, corresponding to O-H stretching due to the presence of the O-H bond in the structure. Additionally, a strong peak related to Fe-O stretching was observed at a wavenumber of approximately 587.0 cm<sup>-1</sup> in the FTIR spectrum. This peak indicates the successfully synthesized of Fe<sub>3</sub>O<sub>4</sub>.

Then, the thermal stability of the adsorbents was assessed using TGA analysis, and the results are shown in Figure 2. Based on the TGA curve, significant weight loss was observed in the temperature range of 31-120°C, gradually increasing from 120-390°C, due to the evaporation and loss of water content from Fe<sub>3</sub>O<sub>4</sub>

structure. This observation is consistent with the findings reported by Mokadem et al. [33]. Furthermore, the results indicated that no significant weight loss occurred at higher temperature (>390°C). Similar trends were reported by Cao et al., where no significant changes were observed in the TGA results near 400°C [34]. Therefore, it can be concluded that Fe<sub>3</sub>O<sub>4</sub> exhibits excellent stability, as only 7% of the weight was decomposed at elevated temperatures [35].

Moreover, VSM was used to investigate the magnetic behavior of the synthesized Fe<sub>3</sub>O<sub>4</sub>. The hysteresis loop of the adsorbents is shown in Figure 3. The Fe<sub>3</sub>O<sub>4</sub> particles exhibited a maximum saturation (Ms) of 135.26 emu/g, indicating a high magnetic strength that falls within the acceptable range for the adsorption process. Additionally, the adsorbents exhibited a superparamagnetic characteristic [20] as evidenced by the S-shaped curved in the hysteresis loop.

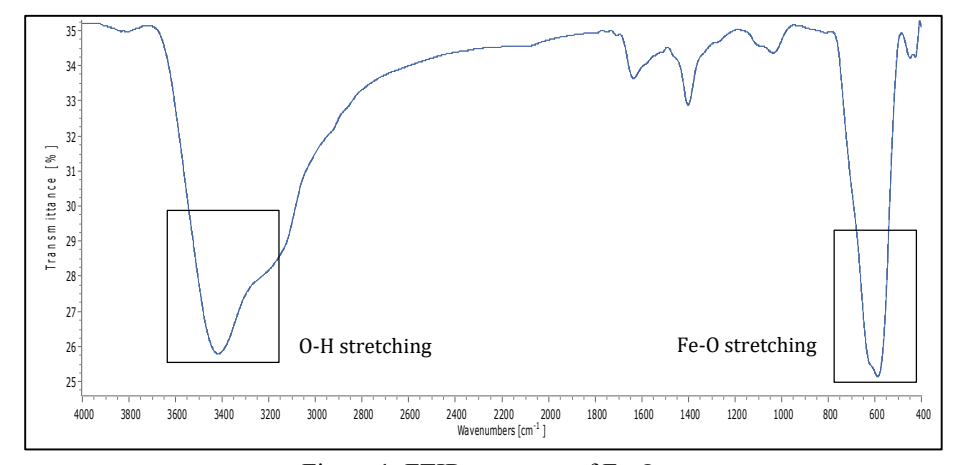


Figure 1. FTIR spectrum of Fe<sub>3</sub>O<sub>4</sub>

Table 4. FTIR frequencies of adsorbents

Characteristics	Fe <sub>3</sub> O <sub>4</sub>
Assignments	Wavenumbers (cm <sup>-1</sup> )
Fe-O stretch	587.0
O-H stretch	3417.6

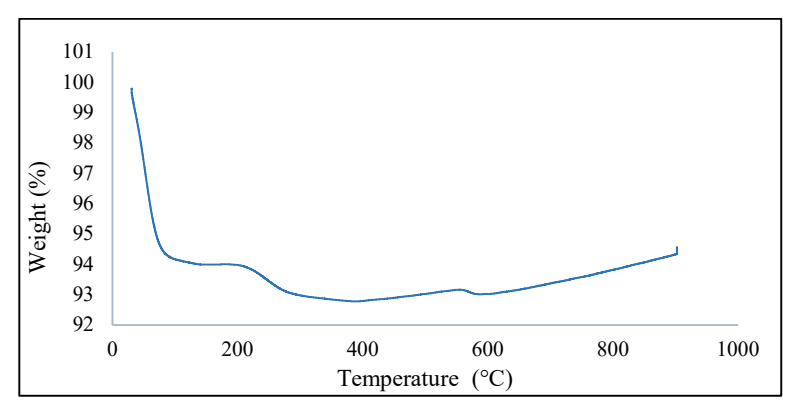


Figure 2. TGA curve of Fe<sub>3</sub>O<sub>4</sub>

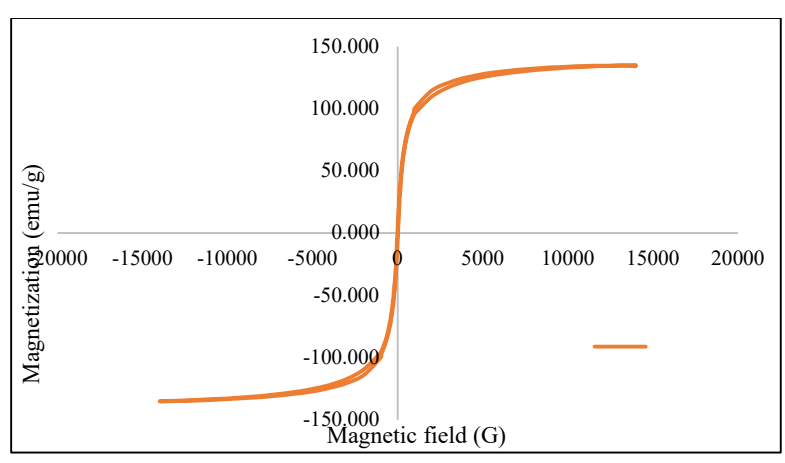


Figure 3. VSM analysis of Fe<sub>3</sub>O<sub>4</sub>

Microscopic morphological analysis of the prepared adsorbents was conducted using TEM and SEM techniques to examine their surface features. TEM images, shown in Figure 4 (a-i), revealed that the particles had an average diameter of approximately 10.42 nm. The Fe<sub>3</sub>O<sub>4</sub> particles were observed to be spherical and uniform in size [36] when captured at various scales ranging from 50 to 500 nm. The images also displayed the aggregation of these small spherical particles into larger aggregates. On the other hand, the SEM image of Fe<sub>3</sub>O<sub>4</sub> depicted in Figure 5, exbibited a beaded, rough, and agglomerated surface structure.

Crystallinity identification was performed using XRD, and the results are plotted in Figure 6. The diffraction peaks of the Fe<sub>3</sub>O<sub>4</sub> exhibited good crystallinity [37]. The solid samples showed diffraction peaks at the  $2\theta$  values of 30.50, 35.73, 43.51, 54.30, 57.30, and 63.04, corresponding to the (220), (311), (400), (422), (511) and (440) cubic spinel planes of Fe<sub>3</sub>O<sub>4</sub> particles, respectively. These values correspond to the joint

committee on powder diffraction standard card number (88-0866 and 19-0629) [36, 37].

The BET surface area of Fe<sub>3</sub>O<sub>4</sub> was found to be 44.6795 m<sup>2</sup>/g. The nitrogen adsorption-desorption isotherm, depicted in Figure 7, indicated that the samples followed a type IV isotherm and exhibited a H3 hysteresis loop. This finding confirmed the mesoporosity of the adsorbents, with pores in the range of 1.5-100 nm [36, 38]. Furthermore, the pore diameters for Fe<sub>3</sub>O<sub>4</sub>. calculated to be approximately 14.44 nm using the Barret-Joyner-Halenda model (BJH), further supported the existence of the adsorbents as mesoporous materials. Mesoporous materials have pore sizes between microporous (< 2 nm) and macroporous (> 50 nm) materials. They offer numerous advantages, such as high surface area, stability, and pore volume. Therefore, Fe<sub>3</sub>O<sub>4</sub>, being in the mesoporous region, exhibited its mesoporosity characteristics, which are beneficial for adsorbate adsorption.

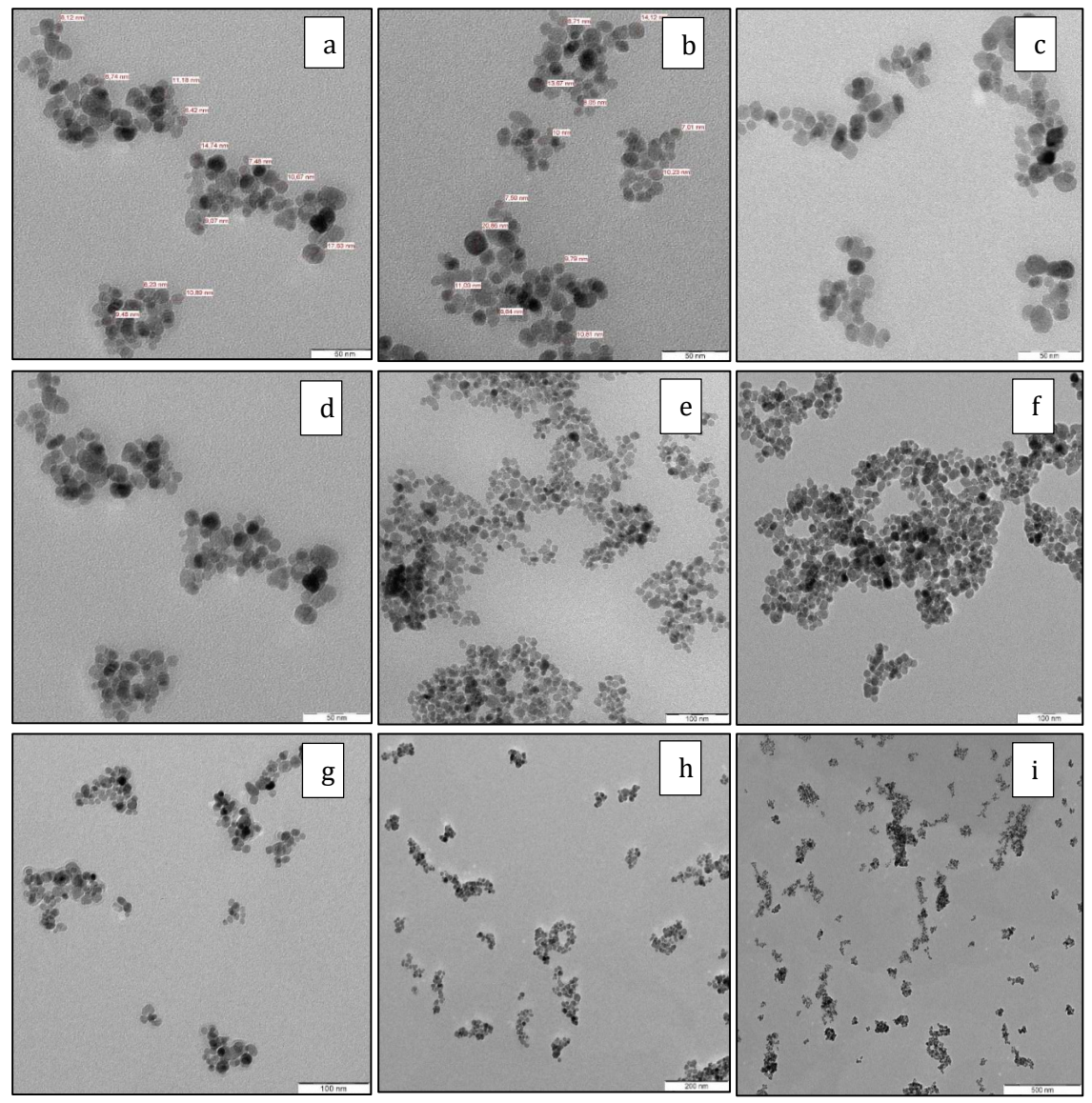


Figure 4. TEM images of  $Fe_3O_4$ . The scale bar at = 50 nm (a-d) 100 nm (e-g) 200 nm (h) 500 (i)

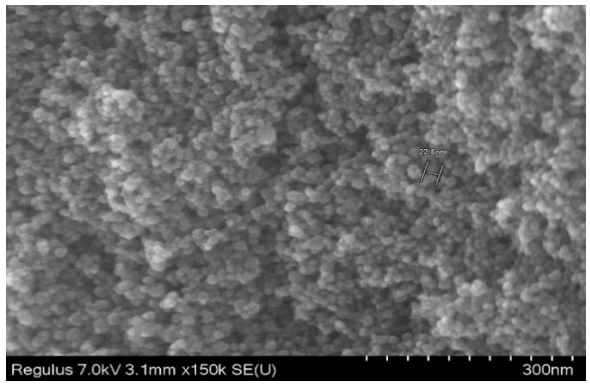


Figure 5. SEM image of Fe<sub>3</sub>O<sub>4</sub>

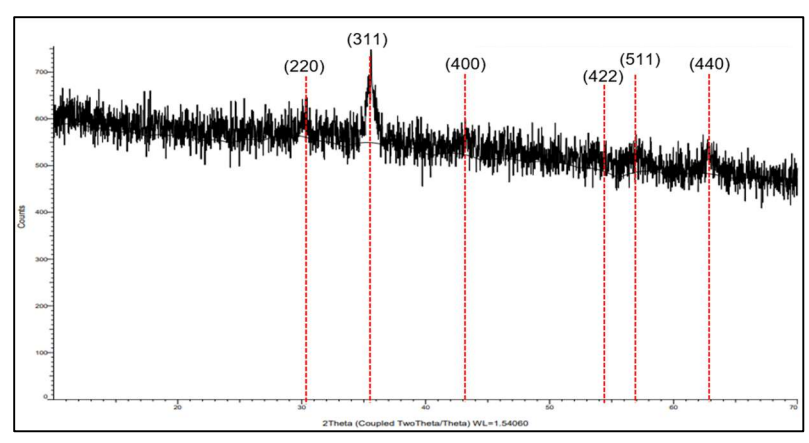


Figure 6. XRD patterns of Fe<sub>3</sub>O<sub>4</sub>

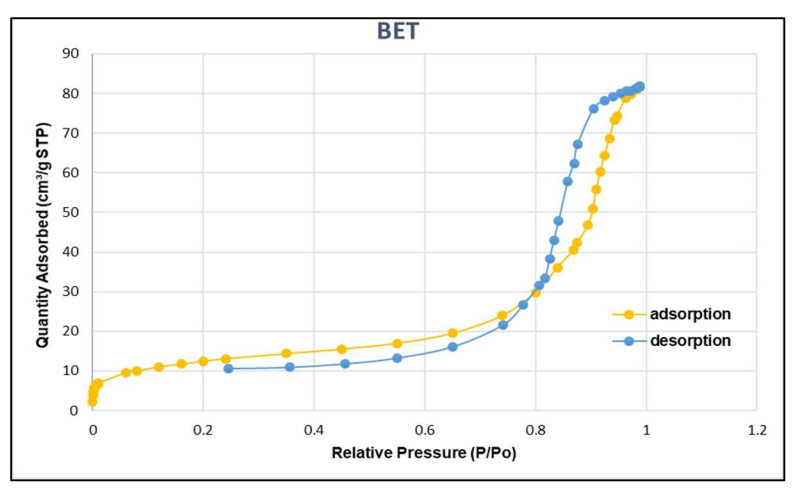


Figure 7. Nitrogen adsorption-desorption isotherm of Fe<sub>3</sub>O<sub>4</sub>

# Optimization for adsorption experiment: Taguchi optimization, the main effect plot for the S/N ratio, and implementation of ANOVA

As mentioned earlier, the Taguchi method was used to optimize three controllable factors: pH, contact period, and adsorbent dosages, with four levels for each factor (testing conditions). Table 5 shows the L<sub>16</sub> orthogonal array design used in this study and the results obtained after each run. The significance order of the controllable factors was determined and is presented in Table 6. The significance order was determined by analyzing the rank of S/N ratio and considering the delta values, which represent the relative magnitude of effects by comparing the highest and lowest average characteristics for each

controllable factor [26, 39].

The results show that the average removal percentage of SY dye (Table 5) ranged from 62.1% to 91.9%, depending on the combination of controllable factors. Additionally, it was observed (Table 6) that the contact period had the most significant variation in the S/N ratio, followed by the adsorbent dosage, and pH. In other words, the contact period had the most significant influence on the adsorption process, while the pH value had the least significant contribution. The optimal conditions for each factor in the adsorption process are also indicated in Table 6.

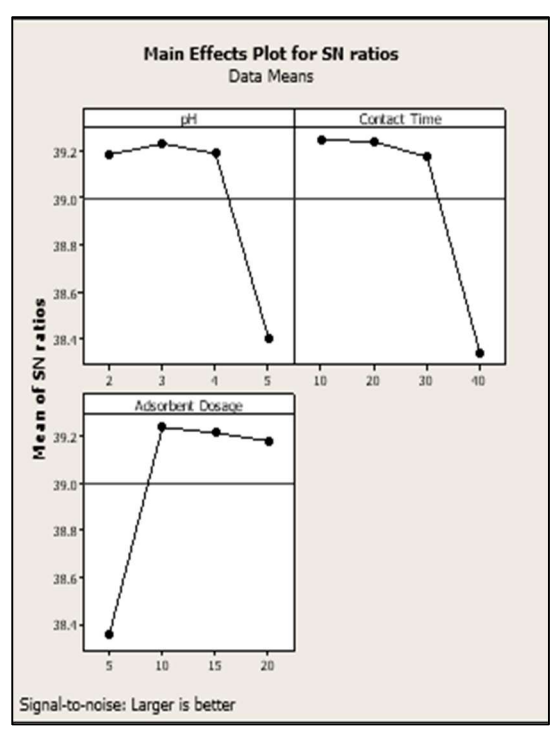


Figure 8. The response curves for the individual effects of SY dye adsorption parameters on S/N ratio

Moreover, the comparative response curves for the independent effects (main effect plot) of the adsorption parameters on the SY removal efficiency can be referred to in Figure 8. Based on the figure, it can be observed that the removal of SY dye increased as the pH increased from 2 to 3. However, the removal trend decreased when the pH value was further increased to 5. The decrease in dye removal can be attributed to the negative charge on adsorbent surface at higher pH [40], which reduces the electrostatic interaction between the dye and the adsorbent surface.

This decrease in removal efficiency is a result of the presence of SY dye as anionic ions (D-SO<sub>3</sub>-) in an aqueous solution, where the sulfonate groups (D-SO<sub>3</sub>Na) of the dye dissociate upon dissolution [41]. Under basic conditions at higher pH value, the adsorbent surface becomes deprotonated and acquires a negative charge. As a result, electrostatic repulsion occurs between the analyte and the adsorbent, leading to a lower removal percentage [20].

A similar study conducted by Rajabi et al. (2015) revealed that the optimal pH for removing SY is 3

because the surface of APTES-modified MNPs has a positive charge in acidic media, which facilitates easier adsorption compared to alkaline pH [42]. This occurs because the surface of modified MNPs tends to attract negatively charged anionic dye molecules. Another study by Bagheri et al. found that the optimal pH for removing SY is 4. The accumulation of SY onto the surface of Fe3O4-MNPs loaded on activated carbon (Fe3O4-MNPs-AC) at a mild pH level can be enhanced by the combination of hydrogen and electrostatic attraction. However, at higher pH levels, the negative and repulsive forces between the anionic dye and the negatively charged adsorbent can hinder the further accumulation of SY on the adsorbent [43]. The trend observed in both studies is similar to the trend observed in our study, where removal of SY is favored at lower pH levels.

Furthermore, a higher pH value resulting from the presence of OH<sup>-</sup> ions from NaOH would also lead to competition with the anionic dye for the active sites of the adsorbent. As a result, the electrostatic interaction between the dye and the adsorbent is reduced due to this competition. In contrast, a lower pH value generates H<sup>+</sup>

ions on the external sites of the adsorbent. This increased the electrostatic interaction between the dye and the nano adsorbents [40], such as Fe<sub>3</sub>O<sub>4</sub>, because the negatively charged dye is attracted to the protonated (positively charged) surface of the adsorbent. Consequently, this enhances their interaction and facilitates the removal process.

However, a slight decrease in dye adsorption was observed below pH 3, which may be attributed to the dissolution of the metal oxide structure. Metal oxides are typically stable over a wide range of pH value, but in extremely acidic solutions, some metal oxides dissolution may occur [2]. This explains the trend line observed in Figure 8, indicating that pH 3 was determined to be the optimal pH condition.

Furthermore, the adsorbent dosage plot exhibited a similar trend line to the pH plot. A significant increase in removal capability was observed when the adsorbent dosage increased from 5 to 10 mg. However, the removal percentage decreased consistently as the adsorbent dosage increased to 20 mg. The initial increase in removal percentage was attributed to the accessibility of active sites, but it eventually became saturated, leading to reduced removal. At higher dosage, the overlapping particles blocked the binding sites, contributing to the decrease in removal ability [40]. Therefore, the trend line observed in Figure 8 indicated that the optimum dosage should be 10 mg. This trend is consistent with studies conducted by Chukwuemeka-Okorie et al. and Sartape et al. for the removal of sunset yellow and malachite green, respectively [45, 44].

The contact time trend was also crucial in determining the removal of SY by Fe<sub>3</sub>O<sub>4</sub>. Based on Figure 8, it can be observed that the removal of SY dye decreased as the contact time increased from 10 to 40 min. This result indicates that the shorter shaking times resulted in more efficient removal due to saturation of the binding sites on Fe<sub>3</sub>O<sub>4</sub>, rendering them unavailable for further adsorption of SY and ultimately reducing the removal rate of the dye. A similar trend was reported in a study by Aziz et el., where the percentage recovery of the analyte decreased with increasing contact time [46].

Moreover, the aqueous suspensions of  $Fe_3O_4$  are generally unstable and can quickly aggregate, limiting their effectiveness [22, 47]. Therefore, the decrease in removal rate with increasing contact time can also attributed to the instability of  $Fe_3O_4$  in the aqueous solution and the subsequently agglomeration of the adsorbent. This hinders the effective of SY dye. Consequently, the trendline would decrease, and in this study, and a contact time 10 min was considered the optimal value, which is adequate for the adsorption process.

Next, ANOVA analysis was conducted to evaluate the contribution of each factor to the efficiency of SY dye removal and to gain a better understanding of the obtained findings and their acceptability within the controllable factors [26, 48]. The ANOVA results are tabulated in Table 7. Based on the results, it can be concluded that the experiments were performed under controlled conditions, as the error value is below 50% contribution [26]. Additionally, the contribution percentage in Table 7 indicate that the contact period had the most significant effect, with the highest contribution percentage, while pH had the least significant effect on SY dye removal by Fe<sub>3</sub>O<sub>4</sub>.

### Effect of temperature and initial concentration of SY dve

Moving on the effect of temperature and initial concentration on SY removal by Fe<sub>3</sub>O<sub>4</sub>, Figure 9 illustrates the binding. In can be observed that the removal percentage increased from 5 ppm to 20 ppm and then decreased as the initial concentration increased to 60 ppm, for all temperatures (298, 313, and 333 K). The initial increase in SY can be attributed to the availability of adsorption sites on the adsorbent and fewer collision between SY molecules, allowing for greater adsorption of analytes at low concentration [49, 50]. However, at higher initial concentrations, the surface area and available adsorption sites available on Fe<sub>3</sub>O<sub>4</sub> became limited compared to the number of dye molecules present [20]. A similar finding was obtained by Aziz et al. for the adsorption of copper (II) onto palm oil boiler mill fly ash (POFA) at different initial concentration [46]. In this study, an initial concentration of 20 ppm was chosen as the optimum concentration for SY dye.

Table 5. Removal of SY dye for each run and S/N ratios

		Contact	Adsorbent	R	Removal (%)			S/N
Run	pН	Time (min)	Dosage (mg)				Removal	
				R1	R2	R3	(%)	Ratio
1	2	10	5	91.8768	91.8349	91.8554	91.8557	39.2621
2	2	20	10	91.5772	91.6026	91.4493	91.5430	39.2325
3	2	30	15	90.9665	90.9170	90.6991	90.8609	39.1675
4	2	40	20	90.1886	89.5809	89.3903	89.7199	39.0576
5	3	10	10	91.6790	91.6889	91.6355	91.6678	39.2443
6	3	20	5	91.6385	91.5604	91.5673	91.5887	39.2368
7	3	30	20	91.3041	91.7280	90.8469	91.2930	39.2085
8	3	40	15	91.4412	91.4764	91.2512	91.3896	39.2179
9	4	10	15	91.5512	91.4914	91.4267	91.4898	39.2274
10	4	20	20	91.4919	91.2922	91.3568	91.3803	39.2170
11	4	30	5	89.0153	89.5729	90.6890	89.7591	39.0608
12	4	40	10	91.5900	91.5293	91.5631	91.5608	39.2342
13	5	10	20	91.6389	91.6059	91.5816	91.6088	39.2387
14	5	20	15	91.7294	91.7031	91.7489	91.7271	39.2500
15	5	30	10	91.7673	91.5475	91.7440	91.6863	39.2461
16	5	40	5	63.8219	60.6472	61.8655	62.1115	35.8577

Table 6. S/N ratios response

		-	1
Level	pН	<b>Contact Period</b>	Adsorbent Dosage
1	39.18	39.24*	38.36
2	39.23*	39.23	39.24*
3	39.18	39.17	39.22
4	38.40	38.34	39.18
Delta	0.83	0.90	0.88
Rank	3	1	2

<sup>\*</sup>The maximum S/N ratio, which indicates the optimum conditions

Table 7. Analysis of Variance

Variance Source	DF	SS	MS	F-ratio	P-value	% Contribution
pН	3	1.921	0.6404	0.89	0.475	18.17
Contact Period	3	2.305	0.7683	1.12	0.381	21.80
Adsorbent Dosage	3	2.213	0.7376	1.06	0.403	20.93
Error	6	4.133	0.6888			39.10
Total	15	10.572				100.00

Regarding the effect of temperature, it was observed that all three temperatures showed nearly identical removal ability. The removal percentage at 298 K, 313 K, and 333 K, as shown in Figure 9, were consistent for each SY concentration. However, at the highest concentration of 60 ppm, the removal percentage at 333 K was slightly

higher than the other two temperatures. This result is consistent with thermodynamics considerations, indicating that the adsorption process is endothermic. Therefore, a temperature 298 K, corresponding to room temperature, was selected as the optimum temperature.

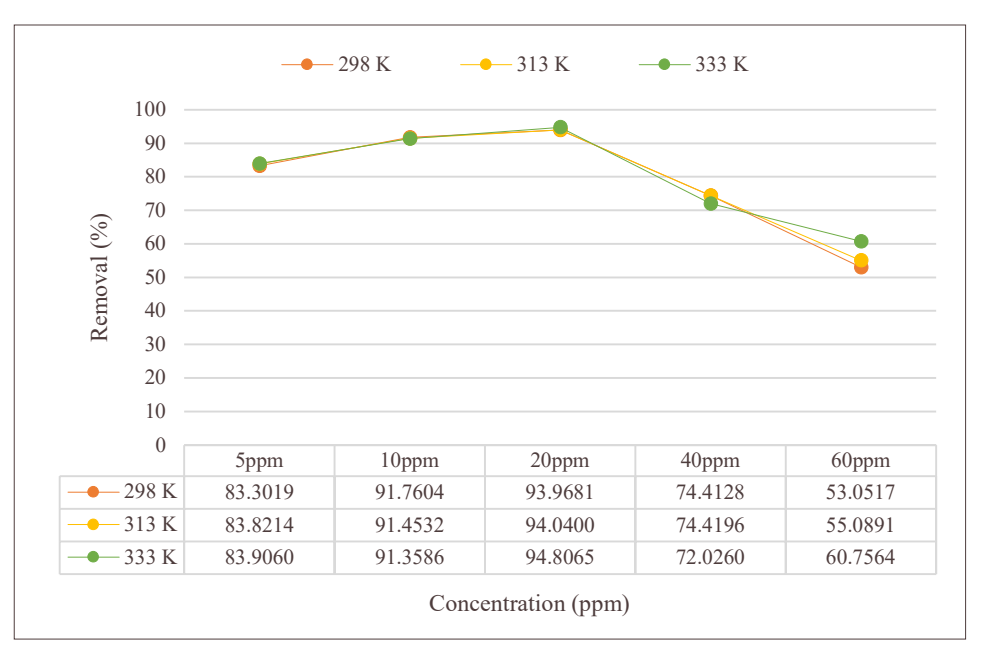


Figure 9. Removal percentage based on initial concentration of SY dye and temperature. Condition: 10 mg of Fe<sub>3</sub>O<sub>4</sub>; contact period: 10 min; pH: 3

#### Adsorption kinetic study

The kinetic study was conducted, and the obtained data was used to plot the y against x curves based on the linear equations of the pseudo-first order (Equation 2) and pseudo-second order (Equation 3). It was observed that the data for the pseudo-second order exhibited the highest R<sup>2</sup> value, approaching one (R<sup>2</sup>= 0.9812). Based on this result, it can be concluded that the adsorption behavior of SY dye onto Fe<sub>3</sub>O<sub>4</sub> followed the pseudo-second order kinetic model. The pseudo-second order curve, along with the linear equation and the R<sup>2</sup> value, can be seen in Figure 10. Additionally, the kinetic

parameters associated with this kinetic model are presented in Table 8.

Furthermore, the validity of the result was confirmed by the close agreement between the calculated  $q_e$  (7.905 mg/g) and the experimental  $q_e$  (9.732 mg/g). The low values of standard deviation and relative error (%) also indicate a better fit of this model to the data. Moreover, the data fitting well with the pseudo-second order suggests that the rate-limiting step involve chemisorption [26], which occurs between the dye and the adsorbent.

Table 8. Pseudo-second order model parameters

Kinetic model	Parameters	Value
Killetic illouei	qe exp (mg/g)	9.732
	qe cal (mg/g)	7.905
	K <sub>2</sub> (g/mg min)	0.041
	h (mg/g min)	2.587
	t <sup>0.5</sup> (min)	0.005
Pseudo-second order	$\mathbb{R}^2$	0.9812
	$\Delta q(\%)$	10.839
	Relative error (%)	18.773

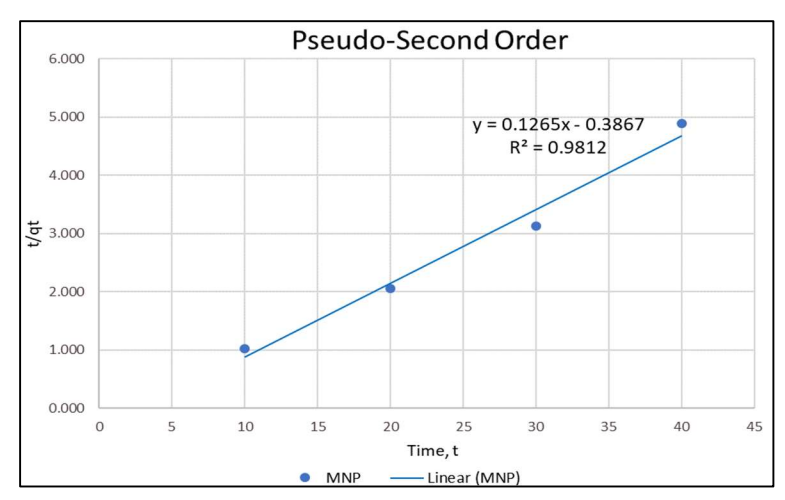


Figure 10. Adsorption kinetic of Sunset Yellow FCF based on pseudo-second order model

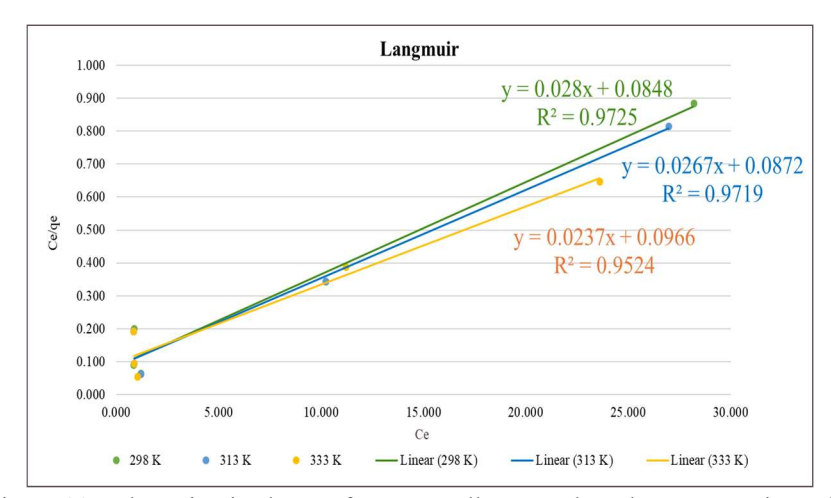


Figure 11. Adsorption isotherm of Sunset Yellow FCF based on Langmuir model

#### Adsorption isotherm study

Furthermore, the isotherm experiment was conducted using several models, and the data obtained was used to plot linear curves based on Equations (6), (7), (8), (10), and (11) for Langmuir, Freundlich, Dubinin-Radusckich, Halsey and Temkin models, respectively. Based on the obtained curved, the Langmuir model exhibited the highest R<sup>2</sup> value, approaching 1. Therefore, it could be concluded that the Langmuir model best fits the data from this study. The curve of this model, along with the calculated parameters, is shown in Figure 11 and Table 9, respectively.

Based on the observed results indicating adherence to the Langmuir model, it suggests that monolayer adsorption occurred, forming a single molecule thickness of adsorbates. Additionally, it validates the homogeneity of the Fe<sub>3</sub>O<sub>4</sub> adsorbent used in this study. Furthermore, the calculated R<sub>L</sub> values in Table 9, obtained using equation (15), indicate that the isotherm adsorption was favorable as all the calculated values between 0 and 1. Thus, it confirmed that Fe<sub>3</sub>O<sub>4</sub> is suitable for the adsorption of SY dye under the conditions employed in this study.

$$R_{L} = \frac{1}{1 + bC_{0}} \tag{15}$$

Where b = Langmuir constant, and  $C_0 = initial concentration of sunset yellow (ppm)$ 

Table 9. Langmuir isotherm model parameters

Isotherm	Domomotoms	Temperature				
Model	Parameters	298 K	313 K	333 K		
Langmuir	q <sub>m</sub> (mg/g)	35.7140	37.4530	42.1940		
	b (L/mg)	0.3300	0.3060	0.2450		
	$\mathbb{R}^2$	0.9725	0.9719	0.9524		
	$R_{ m L}$	0.0481	0.0517	0.0636		

#### Adsorption thermodynamic

Table 10 presents the thermodynamic parameters for the removal of SY dye by  $Fe_3O_4$ . Based on the results, the calculated  $\Delta G^{\circ}$  (J/mol) values in this study were negative. This indicates the spontaneous nature and thermodynamic feasibility [19, 40] of the process at all temperatures. Additionally, the positive value of

enthalpy,  $\Delta H^{\circ}$  (J/mol), suggest that the adsorption process is endothermic. In contrast, the positive entropy value,  $\Delta S^{\circ}$  (J/Kmol), indicates an increase in randomness at the solid/liquid interface during the adsorption process [40, 51]. Furthermore, it suggests a favorable affinity between the adsorbent and the dye [39].

Table 10. Thermodynamic parameters of SY adsorption onto Fe<sub>3</sub>O<sub>4</sub>

Tompovotuvo (V)	$\Delta G^{\circ}$	$\Delta \mathrm{H}^{\circ}$	$\Delta S^{\circ}$
Temperature (K)	(J/mol)	(J/mol)	(J/Kmol)
298	-302.759		
313	-531.646	9.988	42.628
333	-1210.139		

#### Method validation and real sample

To validate the proposed method, the calibration curve of A versus analyte concentration (ranging from 2 to 80 ppm) yielded an R<sup>2</sup> value of 0.9933. The removal percentage and RSD% for inter-day (n=5) and intra-day (n=7) are presented in Table 11. The removal (%) for inter- and intra-day ranged from 34.02% to 82.87% and 33.67% to 82.92%, respectively, while the RSD% for inter-day and intra-day ranged from 2.45% to 6.91% and 2.49% to 6.70%, respectively.

Furthermore, when three real wastewater samples from different locations were spiked with analyte initial concentrations of 5, 20, and 60 ppm, and analyzed using UV–Vis spectrophotometer, the sample removal (%) ranged from 30.10% to 84.43%, with RSD% ranging

from 1.18% to 9.12%, as shown in Table 12. The results indicated that these real wastewater samples had a slightly complicated matrix, as the removal performance was somewhat affected and reduced compared to deionized water, especially at high initial concentrations of the analyte. However, the majority of removal performances achieved high removal percentage, indicating that the Fe<sub>3</sub>O<sub>4</sub> adsorbent was still capable of removing the SY dye from real water samples despite the matrix effect. This suggests that the adsorbent is practical for the removal of sunset yellow dye from wastewater samples. The method can be further developed in the future to improve analyte removal performance.

Table 11. Linearity, repeatability, and precision of the SY dye removal method

Calibration	R <sup>2</sup>	Spiked	Inter-day	Inter-day (n=5)		y (n=7)
Equation		Concentration	Removal	RSD	Removal	RSD
		(ppm)	(%)	(%)	(%)	(%)
		5	82.8634	2.4592	82.9134	2.4943
y = 0.04466x	0.9933	20	56.8058	6.9072	56.8189	6.6933
+ 0.02		60	34.0207	3.3867	33.6763	2.9314

Calibration	R <sup>2</sup>	Spiked	Wastewater A		Wastewater B		Wastewater C	
equation		Concentration (ppm)	Removal	RSD (%)	Removal	RSD (%)	Removal	RSD (%)
		5	82.8634	2.4592	84.4256	2.8177	80.8072	3.0819
y = 0.04466 x + 0.02	0.9933	20	56.8058	6.9072	72.1046	2.7646	53.6209	9.1147
1 0.02		60	34.0207	3.3867	38.9779	4.3579	30.1158	1.1881

Table 12. Three real sample analysis results (Removal% and RSD%)

#### Conclusion

In this study, magnetite or magnetic nanoparticles (MNPs) with the chemical formula Fe<sub>3</sub>O<sub>4</sub>, a basic form of magnetic nanomaterials (MNMs), were successfully synthesized using co-precipitation method. These MNPs were employed as an adsorbent for the removal of sunset yellow FCF dye from aqueous samples. Various instruments such as VSM, TGA, FTIR, SEM, TEM, XRD, and BET were utilized to investigate the physical characteristics of the prepared adsorbents, including their properties, structures, surface areas, and functional groups.

To determine the optimized conditions for the removal of SY dye by Fe<sub>3</sub>O<sub>4</sub>, an adsorption study was conducted. The Taguchi method was employed for the optimization experiments, and the optimal testing conditions were found to be pH 3, 10 mg adsorbent dose, and 10 min contact time. Additionally, when the optimization for the effect of temperature and initial concentration of the dye was carried out separately, the optimum initial concentration of the dye was observed to be 20 ppm. Furthermore, room temperature was chosen as the optimum temperature, as consistent results were obtained across the all-tested temperatures. The application of these optimized conditions in further adsorption studies revealed that the kinetics behavior of the adsorbents towards SY dye followed the pseudosecond order model, while the isotherm study showed good fit with the Langmuir model. This indicates a chemical interaction or chemisorption between the adsorbents and adsorbate molecules, forming a monolayer adsorption. Moreover, the adsorption study demonstrated feasibility, endothermic nature, and spontaneous occurrence with increasing randomness.

Subsequently, the real wastewater samples from three different areas were used for method validation and real

sample analysis. These samples were spiked with three different concentrations of analytes. The removal percentage ranged from 30% to 85%, with a low range of RSD% (1.8% to 9.2%). This suggests that the proposed adsorbent could effectively remove SY dye from real wastewater samples, albeit with slight influence from the matrix effect. Therefore, this study provides valuable insights into the nature of Fe3O4 and confirms the validity and practicality of the proposed method for removing SY dye from real wastewater samples. Further comprehensive studies can be conducted to enhance the removal performance.

#### Acknowledgements

The authors would like to express their gratitude to the Ministry of Higher Education, Malaysia for providing funding for this project through the Fundamental Research Grant Scheme (FRGS) with reference code FRGS/1/2021/STG04/USM/02/8 and account code 203.CIPPT.6711974. The authors are also thankful to the Advanced Medical and Dental Institute, Universiti Sains Malaysia, for providing the necessary resources to complete this project.

#### References

- Jeeva, M., Lakkaboya, S. K., and Wan Zuhairi, W. Y. (2019). The adsorption of direct brown 1 dye using kaolinite and surfactant modified kaolinite. Bulletin of the Geological Society of Malaysia, 2019(67): 35-45.
- Xiao, W., Jiang, X., Liu, X., Zhou, W., Garba, Z. N., Lawan, I., Wang, L., and Yuan, Z. (2021). Adsorption of organic dyes from wastewater by metal-doped porous carbon materials. *Journal of Cleaner Production*, 284: 124773.
- 3. Lu, Y., Song, S., Wang, R., Liu, Z., Meng, J., Sweetman, A. J., Jenkins, A., Ferrier, R. C., Li, H., Luo, W., and Wang, T. (2015). Impacts of soil and

- water pollution on food safety and health risks in China. *Environment International*, 77: 5-15.
- Ma, X., Liu, Y., Li, X., Xu, J., Gu, G., and Xia, C. (2015). Water: The most effective solvent for liquid-phase hydrodechlorination of chlorophenols over Raney Ni catalyst. *Applied Catalysis B: Environmental*, 165: 351-359.
- Belachew, N., and Hinsene, H. (2020). Preparation of cationic surfactant-modified kaolin for enhanced adsorption of hexavalent chromium from aqueous solution. *Applied Water Science*, 10(1): 38.
- Foroughirad, S., Haddadi-Asl, V., Khosravi, A., and Salami-Kalajahi, M. (2020f). Synthesis of magnetic nanoparticles-decorated halloysite nanotubes/poly([2-(acryloyloxy)ethyl]trimethylammonium chloride) hybrid nanoparticles for removal of Sunset Yellow from water. *Journal of Polymer Research*, 27(10): 320.
- Mosayebian, M. B. and Reza Moradi, K. M. (2021). Modelling the degradation of sunset yellow FCF azo dye by Fe<sub>2</sub>O<sub>3</sub>/Bentonite catalyst using artificial neural networks. *Journal of Nanoanalysis*, 8(3): 209-220.
- Rovina, K., Acung, L. A., Siddiquee, S., Akanda, J. H., and Shaarani, S. M. (2017h). Extraction and analytical methods for determination of sunset yellow (E110)—a review. *Food Analytical Methods*, 10: 773-787.
- Gholami, Z., Marhamatizadeh, M. H., Yousefinejad, S., Rashedinia, M., and Mazloomi, S. M. (2021). Vortex-assisted dispersive liquid-liquid microextraction based on hydrophobic deep eutectic solvent for the simultaneous identification of eight synthetic dyes in jellies and drinks using HPLC-PDA. Microchemical Journal, 170: 106671.
- 10. El-Borm, H., Badawy, G., Hassab El-Nabi, S., El-Sherif, W., and Atallah, M. (2020). Toxicity of sunset yellow FCF and tartrazine dyes on DNA and cell cycle of liver and kidneys of the chick embryo: the alleviative effects of curcumin. *Egyptian Journal of Zoology*, 74(74): 43-55.
- Rovina, K., Siddiquee, S., and Shaarani, S. M. (2016k). Highly sensitive determination of sunset yellow FCF (E110) in food products based on chitosan/nanoparticles/MWCNTs with modified

- gold electrode. *IOP Conference Series: Earth and Environmental Science*, 36(1): 012023.
- Nwuzor, I. C., Chukwuneke, J. L., Nwanoneyi, S. C., Obasi, H. C., and Ihekweme, G. O. (2018). Modification and Physiochemical Characterization of Kaolin Clay for Adsorption of Pollutants from Industrial Paint Effluent. European Journal of Advances in Engineering and Technology, 5(8): 609-620.
- Villar Blanco, L., González Sas, O., Sánchez, P. B., Domínguez Santiago, Á., and González de Prado, B. (2022). Congo red recovery from water using green extraction solvents. Water Resources and Industry, 27: 100170.
- 14. El Mouhri, G., Merzouki, M., Belhassan, H., Miyah, Y., Amakdouf, H., Elmountassir, R., and Lahrichi, A. (2020). Continuous adsorption modelling and fixed bed column studies: Adsorption of tannery wastewater pollutants using beach sand. *Journal of Chemistry*, 2020: 7613484.
- Benjelloun, M., Miyah, Y., Akdemir Evrendilek, G., Zerrouq, F., and Lairini, S. (2021). Recent advances in adsorption kinetic models: Their application to dye types. *Arabian Journal of Chemistry*, 14(4): 103031.
- Lawal, I. A., Lawal, M. M., Azeez, M. A., and Ndungu, P. (2019). Theoretical and experimental adsorption studies of phenol and crystal violet dye on carbon nanotube functionalized with deep eutectic solvent. *Journal of Molecular Liquids*, 288: 110895.
- Panda, S. K., Aggarwal, I., Kumar, H., Prasad, L., Kumar, A., Sharma, A., Vo, D. V. N., Van Thuan, D., and Mishra, V. (2021). Magnetite nanoparticles as sorbents for dye removal: A review. *Environmental Chemistry Letters*, 19(3): 2487-2525.
- Soliman, N. K., and Moustafa, A. F. (2020). Industrial solid waste for heavy metals adsorption features and challenges: A review. *Journal of Materials Research and Technology*, 9(5): 10235-10253.
- Husin, N. A., Muhamad, M., Yahaya, N., Miskam, M., Syazni Nik Mohamed Kamal, N. N., Asman, S., Raoov, M., and Mohamad Zain, N. N. (2021). Application of a new choline-imidazole based deep

- eutectic solvents in hybrid magnetic molecularly imprinted polymer for efficient and selective removal of naproxen from aqueous samples. *Materials Chemistry and Physics*, 261: 124228.
- 20. Husin, N. A., Hashim, N. M., Yahaya, N., Miskam, M., Raoov, M., and Zain, N. N. M. (2021). Exploring magnetic particle surface embedded with imidazole-based deep eutectic solvent for diclofenac removal from pharmaceutical wastewater samples. *Journal of Molecular Liquids*, 332: 115809.
- Rodríguez-Ramos, R., Santana-Mayor, Á., Socas-Rodríguez, B., and Rodríguez-Delgado, M. Á. (2021). Recent applications of deep eutectic solvents in environmental analysis. *Applied Sciences (Switzerland)*, 11(11): 11114779.
- 22. Wei, X., Wang, Y., Chen, J., Xu, P., Xu, W., Ni, R., Meng, J., and Zhou, Y. (2019). Poly(deep eutectic solvent)-functionalized magnetic metal-organic framework composites coupled with solid-phase extraction for the selective separation of cationic dyes. *Analytica Chimica Acta*, 1056: 47-61.
- Badu Latip, N. M., Gopal, K., Suwaibatu, M., Hashim, N. M., Rahim, N. Y., Raoov, M., Yahaya, N., and Mohamad Zain, N. N. (2021). Removal of 2,4-dichlorophenol from wastewater by an efficient adsorbent of magnetic activated carbon. Separation Science and Technology (Philadelphia), 56(2): 252-265.
- Rezaei, H., Haghshenasfard, M., and Moheb, A. (2017). Optimization of dye adsorption using Fe<sub>3</sub>O<sub>4</sub> nanoparticles encapsulated with alginate beads by Taguchi method. *Adsorption Science and Technology*, 35(1–2): 55-71.
- 25. Nandhini, M., Suchithra, B., Saravanathamizhan, R., and Prakash, D. G. (2014). Optimization of parameters for dye removal by electro-oxidation using Taguchi design. *Journal of Electrochemical Science and Engineering*, 4(4): 227-234.
- Korake, S. R., and Jadhao, P. D. (2021). Investigation of Taguchi optimization, equilibrium isotherms, and kinetic modeling for cadmium adsorption onto deposited silt. *Heliyon*, 7(1): e05755.
- 27. Wang, J., and Guo, X. (2020). Adsorption kinetic models: Physical meanings, applications, and

- solving methods. *Journal of Hazardous Materials*, 390: 122156.
- 28. Ebelegi, A. N., Ayawei, N., and Wankasi, D. (2020ab). Interpretation of adsorption thermodynamics and kinetics. *Open Journal of Physical Chemistry*, 10(03): 166-182.
- 29. Chen, X. (2015). Modelling of experimental adsorption isotherm data. *Information* (Switzerland), 6(1): 14-22.
- 30. Al-Ghouti, M. A., and Da'ana, D. A. (2020). Guidelines for the use and interpretation of adsorption isotherm models: A review. *Journal of Hazardous Materials*, 393: 122383.
- 31. Al-Khateeb, L. A., Hakami, W., and Salam, M. A. (2017). Removal of non-steroidal anti-inflammatory drugs from water using high surface area nanographene: Kinetic and thermodynamic studies. *Journal of Molecular Liquids*, 241: 733-741.
- 32. Thaligari, S. K., Srivastava, V. C., and Prasad, B. (2016). Adsorptive desulfurization by zincimpregnated activated carbon: characterization, kinetics, isotherms, and thermodynamic modelling. *Clean Technologies and Environmental Policy*, 18(4): 1021-1030.
- 33. Mokadem, Z., Mekki, S., Saïdi-Besbes, S., Agusti, G., Elaissari, A., and Derdour, A. (2017). Triazole containing magnetic core-silica shell nanoparticles for Pb<sup>2+</sup>, Cu<sup>2+</sup> and Zn<sup>2+</sup> removal. *Arabian Journal of Chemistry*, 10(8): 1039-1051.
- 34. Cao, H., He, J., Deng, L., and Gao, X. (2009). Fabrication of cyclodextrin-functionalized superparamagnetic Fe<sub>3</sub>O<sub>4</sub> /amino-silane core-shell nanoparticles via layer-by-layer method. *Applied Surface Science*, 255(18): 7974-7980.
- 35. Hashim, N. M., Mohamad, M., Kamal, N. N. S. N. M., Aziz, M. Y., Mohamad, S., Yahaya, N., and Zain, N. N. M. (2023). Revolutionizing drug removal: Green magnetic nanoparticles functionalized with hydrophobic deep eutectic solvents for anti-inflammatory drug adsorption. *Journal of Molecular Liquids*, 383: 122082.
- 36. Mamman, S., Suah, F. B. M., Raaov, M., Mehamod, F. S., Asman, S., and Zain, N. N. M. (2021). Removal of bisphenol A from aqueous media using a highly selective adsorbent of hybridization

- cyclodextrin with magnetic molecularly imprinted polymer. Royal Society Open Science, 8(3): 201604
- 37. Shahriman, M. S., Mohamad Zain, N. N., Mohamad, S., Abdul Manan, N. S., Yaman, S. M., Asman, S., and Raoov, M. (2018). Polyaniline modified magnetic nanoparticles coated with dicationic ionic liquid for effective removal of rhodamine B (RB) from aqueous solution. RSC Advances, 8(58): 33180–33192.
- 38. Meftah Elgubbi, H., Salhah Othman, S., and Wahida Harun, F. (2020). Modification of kaolinite clay using benzyltriethylammonium chloride as a surfactant: Preparation and characterization. *International Journal of Engineering & Technology*, 9(4): 31088.
- 39. Mosoarca, G., Popa, S., Vancea, C., and Boran, S. (2021). Optimization, equilibrium and kinetic modeling of methylene blue removal from aqueous solutions using dry bean pods husks powder. *Materials*, 14(19): 14195673.
- Noreen, S., Mustafa, G., Ibrahim, S. M., Naz, S., Iqbal, M., Yaseen, M., Javed, T., and Nisar, J. (2020). Iron oxide (Fe<sub>2</sub>O<sub>3</sub>) prepared via green route and adsorption efficiency evaluation for an anionic dye: Kinetics, isotherms and thermodynamics studies. *Journal of Materials Research and Technology*, 9(3): 4206-4217.
- 41. De Sá, F. P., Cunha, B. N., and Nunes, L. M. (2013). Effect of pH on the adsorption of sunset yellow FCF food dye into a layered double hydroxide (CaAl-LDH-NO<sub>3</sub>). *Chemical Engineering Journal*, 215–216: 122-127.
- 42. Rajabi, H. R., Arjmand, H., Hoseini, S. J., and Nasrabadi, H. (2015). Surface modified magnetic nanoparticles as efficient and green sorbents: Synthesis, characterization, and application for the removal of anionic dye. *Journal of Magnetism and Magnetic Materials*, 394: 7-13.
- 43. Bagheri, A. R., Ghaedi, M., Asfaram, A., Bazrafshan, A. A., and Jannesar, R. (2017). Comparative study on ultrasonic assisted adsorption of dyes from single system onto Fe3O4 magnetite nanoparticles loaded on activated carbon: Experimental design methodology. *Ultrasonics Sonochemistry*, 34: 294-304.

- 44. Chukwuemeka-Okorie, H. O., Ekuma, F. K., Akpomie, K. G., Nnaji, J. C., and Okereafor, A. G. (2021). Adsorption of tartrazine and sunset yellow anionic dyes onto activated carbon derived from cassava sievate biomass. *Applied Water Science*, 11(2): 27.
- 45. Sartape, A. S., Mandhare, A. M., Jadhav, V. V., Raut, P. D., Anuse, M. A., and Kolekar, S. S. (2017). Removal of malachite green dye from aqueous solution with adsorption technique using *Limonia acidissima* (wood apple) shell as low-cost adsorbent. *Arabian Journal of Chemistry*, 10: 3229-3238.
- 46. Aziz, A. S. A., Manaf, L. A., Man, H. C., and Kumar, N. S. (2014). kinetic modeling and isotherm studies for copper(II) adsorption onto palm oil boiler mill fly ash (POFA) as a natural low-cost adsorbents. *BioResources*, 9(1): 336-356.
- 47. Marć, M., Drzewiński, A., Wolak, W. W., Najder-Kozdrowska, L., and Dudek, M. R. (2021). Filtration of nanoparticle agglomerates in aqueous colloidal suspensions exposed to an external radio-frequency magnetic field. *Nanomaterials*, 11(7):1737
- 48. Madan, S. S., and Wasewar, K. L. (2017). Optimization for benzeneacetic acid removal from aqueous solution using CaO<sub>2</sub> nanoparticles based on Taguchi method. *Journal of Applied Research and Technology*, 15(4): 332-339.
- 49. Oetjik, W., and Aida Ibrahim, S. (2021). A review: The effect of initial dye concentration and contact time on the process of dye adsorption using agricultural wastes adsorbent. *Progress in Engineering Application and Technology*, 2(2): 2773-5303.
- Panda, H., Tiadi, N., Mohanty, M., and Mohanty, C. R. (2017). Studies on adsorption behavior of an industrial waste for removal of chromium from aqueous solution. South African Journal of Chemical Engineering, 23: 132-138.
- 51. Javadian, H., Koutenaei, B. B., Shekarian, E., Sorkhrodi, F. Z., Khatti, R., and Toosi, M. (2017). Application of functionalized nano HMS type mesoporous silica with N-(2-aminoethyl)-3-aminopropyl methyldimethoxysilane as a suitable adsorbent for removal of Pb(II) from aqueous

### Mohd Husani et al.: MAGNETIC NANOPARTICLE FOR REMOVING SUNSET YELLOW DYE: TAGUCHI OPTIMIZATION

media and industrial wastewater. *Journal of Saudi Chemical Society*, 21: 219-230